Ab initio study of MnO and NiO

M. D. Towler and N. L. Allan

School of Chemistry, Bristol University, Cantock's Close, Bristol BS8 1TS, United Kingdom

N. M. Harrison and V. R. Saunders

Daresbury Laboratory, Science and Engineering Research Council, Daresbury, Warrington, Cheshire WA4 4AD, United Kingdom

W. C. Mackrodt

Department of Theoretical Chemistry, Oxford University, 5, South Parks Road, Oxford OX1 3UB, United Kingdom

E. Aprà

Department of Inorganic, Physical and Materials Chemistry, University of Torino, via Giuria 5, I-10125 Torino, Italy

The ground-state electronic structure of NiO and MnO has been calculated within the Hartree-Fock approximation using local Gaussian basis sets. For both, a qualitatively correct ground-state electronic structure is obtained in which the wide-band-gap insulating character of these materials is seen to be a result of large on-site Coulomb interactions. The materials are correctly predicted to be antiferromagnetic with the AF_2 structure. The relative energy differences between various magnetic structures are consistent with the ratio of the Néel temperatures. The structural, elastic, and vibrational properties are in reasonable agreement with available experimental data.

I. INTRODUCTION

Since their unusual insulating and magnetic properties were first recognized in the 1930s, the first-row transition-metal monoxides have provided considerable challenges to commonly accepted theories of electronic structure and bonding. In this paper we consider MnO and NiO, which crystallize in the rock-salt structure and which at low temperatures are found to be high-spin anti-ferromagnetic insulators with conductivities[1,2] in the range $10^{-15}-10^{-17}$ Ω^{-1}cm^{-1} and Néel temperatures (T_N) of 116 and 525 K, respectively.[3] The insulating character and local magnetic moments of both are maintained above T_N, with optical band gaps of 3.6 and 3.8 eV which are essentially independent of T. This is in marked contrast to many materials which undergo metal-insulator transitions such as VO_2, NiS, and V_2O_3, where the optical gaps are all less than 0.6 eV and decrease markedly with increasing temperature. The persistence of the insulating gap and local moments above the spin-disordering temperature appears to be the best phenomenological way of defining the Mott-insulator state, although a recent development has been the differentiation between Mott-Hubbard and charge-transfer insulators, based on whether the observed gap is of $d \rightarrow d$ or $p \rightarrow d$ character.[4,5]

The majority of previous theoretical treatments of the transition metal oxides have been based on the local-spin-density approximation (LSDA), which encounters serious problems in describing such cases.[6,7] The work of Brandow[8–10] and others has suggested that a useful model for Mott insulators is provided by unrestricted

Hartree-Fock (UHF) theory. Indeed, the most recent density-functional calculations have tended to include modifications such as self-interaction-corrected (SIC) LSDA (Ref. 11) and LSDA+U (Ref. 12) in an apparent attempt to emulate features of the Hartree-Fock Hamiltonian. These studies have offered improved descriptions of the Mott-insulating state.

In the present work, therefore, we apply the *ab initio* linear-combination of atomic orbitals (LCAO) periodic Hartree-Fock approach, embodied in the CRYSTAL92 code,[13,14] to MnO and NiO using extended basis sets and the UHF scheme for describing open shell states.[15] This scheme has been used previously to examine a range of other oxides, including Li_2O,[16,17] MgO,[18] and Al_2O_3.[19,20] Preliminary results from a study of the ground-state properties of a selection of the first-row monoxides, including CaO and the metallic oxide VO, have been presented in a previous paper.[21] In this work we provide a much more detailed study of MnO and NiO and extend the treatment previously given to include elastic properties and phonon frequencies. We are aware of only two previous *ab initio* Hartree-Fock studies of these materials, one due to Kunz,[2] the other to Janssen and Nieuwpoort,[22] who consider a $[NiO_6]^{10-}$ cluster in a point ion field.

Recent experimental and theoretical evidence has led to the speculation that the upper valence band in these materials is primarily O $2p$ in character.[11,22–27] This has important consequences regarding both the nature of hole states and the valency of the higher oxides, and has led to the suggested classification of NiO as a charge-transfer insulator.[4,5]

The structure of the present paper is as follows. In Sec. II some general points will be made regarding methodology and the local basis sets used. In Sec. III a wide range of results for MnO and NiO are presented including the calculated lattice structure, magnetostriction, magnetic moments, Néel temperatures, band structure, density of states, charge density, elastic constants, and phonon frequencies. The electronic structure is analyzed in terms of a single site model.[8-10]

II. COMPUTATIONAL METHOD

The implementation of the all-electron *ab initio* self-consistent field (SCF) Hartree-Fock LCAO computational scheme for periodic systems within the computer code CRYSTAL92 has been described previously.[13,14] There are a number of limitations to the accuracy of calculations using this scheme. The main source of error (electron correlation) stems directly from the Hartree-Fock approximation. In previous work, this has generally led to an underestimate of the binding energies by about 30%, and to overestimates of the lattice parameter by approxi-

mately 2%, although successful attempts have been made to include correlation corrections using functionals of the Hartree-Fock density.[28]

The second inaccuracy stems from numerical approximations introduced in the implementation of the SCF equations. These approximations appear in the reciprocal space integration to reconstruct the electronic charge distribution and in the evaluation of the Coulomb and exchange series. In these series, the Gaussian integrals are classified according to overlap or penetration criteria. Integrals of sufficiently low overlap or penetration may be neglected or approximated, the cutoffs being controlled by five parameters. Our calculations were performed with these tolerances set to 10^{-6}, 10^{-8}, 10^{-7}, 10^{-6}, and 10^{-14}, which provide high numerical accuracy. The detailed effect of these parameters is discussed elsewhere.[29] The reciprocal space integration[30] was performed by sampling the Brillouin zone at a regular set of points defined by a shrinking factor of 8. Errors are greatest for numerically evaluated second derivatives; we estimate that the numerical error is less than 2% for elastic constants and phonon frequencies and negligible for the lattice structure.

TABLE I. Core and valence basis sets for MnO and NiO.

No.	Shell type	Mn Exponent	Mn Coefficients		Ni Exponent	Ni Coefficients		O Exponent	O Coefficients	
				Core bases						
1	s	292 601.0	0.000 227		367 916.0	0.000 227		8020.0	0.001 08	
		42 265.0	0.001 9		52 493.9	0.001 929		1338.0	0.008 04	
		8 947.29	0.011 1		11 175.8	0.011 1		255.4	0.053 24	
		2 330.32	0.050 1		2 925.4	0.050 0		69.22	0.168 1	
		702.047	0.170 5		882.875	0.170 3		23.90	0.358 1	
		242.907	0.369 1		305.538	0.369 0		9.264	0.385 5	
		94.955	0.403 5		119.551	0.403 5		3.851	0.146 8	
		39.5777	0.143 7		49.9247	0.142 6		1.212	0.072 8	
2	sp	732.14	−0.0053	0.0086	924.525	−0.0052	0.0086	49.43	−0.008 83	0.009 58
		175.551	−0.0673	0.0612	223.044	−0.0679	0.0609	10.47	−0.091 5	0.069 6
		58.5093	−0.1293	0.2135	74.4211	−0.1319	0.2135	3.235	−0.040 2	0.206 5
		23.129	0.2535	0.4018	29.6211	0.2576	0.3944	1.217	0.379 0	0.347 0
		9.7536	0.6345	0.4012	12.4721	0.6357	0.3973			
		3.4545	0.2714	0.2222	4.2461	0.2838	0.2586			
3	sp	38.389	0.0157	−0.0311	56.6581	0.0124	−0.0180			
		15.4367	−0.2535	−0.0969	21.2063	−0.2218	−0.0800			
		6.1781	−0.8648	0.2563	8.4914	−0.8713	0.2089			
		2.8235	0.9337	1.6552	3.6152	1.0285	1.2550			
				Valence bases						
4	sp	1.2086	1.0	1.0	1.5145	1.0	1.0	0.4980[a]	1.0	1.0
5	sp	0.4986	1.0	1.0	0.6144	1.0	1.0	0.1690[a]	1.0	1.0
6	d	22.5929	0.0708		41.0800[b]	0.0405				
		6.1674	0.3044		11.4130[b]	0.2022				
		2.0638	0.5469		3.8561[b]	0.4338				
		0.7401	0.5102		1.3302[b]	0.4897				
7	d	0.2490	1.0		0.4110	1.0				

[a]These are from an original CaO oxygen basis (Ref. 21). Optimized values for MnO are 0.4763 and 0.1760 $bohr^{-2}$ and for NiO 0.4764 and 0.1802 $bohr^2$.
[b]Given incorrectly in our previous paper (Ref. 21).

The final source of error relates to the choice of basis set. Extended Gaussian basis sets were generated for both oxides composed of 27 atomic orbitals for Mn and Ni and 13 for oxygen, where each orbital is a linear combination (contraction) of Gaussian-type functions. The basis sets were derived in the following manner. Complete sets of contraction coefficients and exponents for the cation bases were obtained by energy minimization of the free-ion +2 state. Together with a previously derived basis set for oxygen in CaO,[21] the free-ion bases were then used to derive a basis set appropriate for a description of the solid state by minimizing the ground-state energy of the solid in a single unit-cell description at the experimental lattice constants.[31] The exponents and contraction coefficients for the cation d shells and for the two outermost sp shells of the cation and oxygen bases were optimized in this way. The final part of the procedure involved optimizing the geometry and the same basis set parameters in turn until self-consistency was achieved. The basis sets adopted are given in Table I.

III. RESULTS

A. Geometry and magnetic properties

In the observed low-temperature antiferromagnetic state the individual atomic moments of MnO and NiO are aligned in ferromagnetic (111) sheets, with adjacent sheets having antiparallel spin. This is generally referred to as the AF_2 spin arrangement. In Table II we list the calculated equilibrium lattice constants for this state and compare these with the available x-ray data. For comparison, predicted geometries using the same basis sets are given for the hypothetical ferromagnetic and AF_1 magnetic states, where the latter consists of (100) ferromagnetic sheets with adjacent sheets antiparallel. These calculations were all performed by minimization of the total energy of cells containing two formula units. For both systems the calculated lattice constants are around 2% greater than the experimental values, which is typical of previous studies of closed-shell oxides.[16,17−20,28] Table II also contains a comparison of Hartree-Fock binding energies, derived from the difference between the crystal and atomic solutions, and the corresponding experimental values. The underestimate of approximately 30% due to the neglect of the

electron correlation is again compatible with earlier work.[28]

Calculated and experimental magnetic moments are compared in Table III. The calculated values are deduced from Mulliken population analyses of the UHF wave function. Our values for MnO and NiO, $4.92\mu_B$ and $1.92\mu_B$, may be compared with SIC-LSD values of $4.49\mu_B$ and $1.53\mu_B$, respectively, calculated by Svane and Gunnarsson.[11] The inclusion of correlation effects would tend to decrease our predicted moments, whereas spin-orbit coupling (which is neglected) will tend to increase the moments. However, perhaps a more useful comparison would be between experimental and theoretical neutron-scattering factors.[21]

The relative energies of the closed-shell and various ferromagnetic states (differing in their magnetic moments) at the calculated ground-state lattice constants are shown in Table IV. From these it is clear that Hartree-Fock calculations correctly predict both MnO and NiO to be high-spin insulators. The relative stability of the antiferromagnetic and ferromagnetic states are reported in Table V at the calculated ground-state lattice constants. The AF_2 state is correctly predicted to be the most stable spin configuration followed by the ferromagnetic and then the AF_1. Furthermore this order does not change when calculations are performed at the optimal geometry of either of the latter two configurations. We can write the energy difference between any two magnetic states in the form $\Delta n E_{se} + \Delta n' E_{de}$, where E_{se} and E_{de} refer to contributions from second-neighbor superexchange and first-neighbor direct exchange, respectively. Δn and $\Delta n'$ are the differences in the number of such interactions between the two states. Given the energy differences listed in Table V it is straightforward to estimate values of E_{se} and E_{de} for MnO and NiO. For MnO, E_{se} and E_{de} are -2.0×10^{-3} and -5.0×10^{-5} eV, respectively; the corresponding values for NiO are -7.0×10^{-3} and -1.5×10^{-3} eV. As expected, $|E_{se}| > |E_{de}|$ for both compounds.

In preliminary work,[32] using a pseudopotential model to represent the core electron distribution in the transition-metal ions, the variation of the energy difference ΔE_{stab} between the ferromagnetic and antiferromagnetic (AF_2) solutions as a function of lattice parameter was investigated. On increasing the cation-anion separation, ΔE_{stab} decreases markedly due to the reduced M-O-M superexchange interaction. At very high lattice parameters, the effects of ordinary exchange increasingly favor the pairing of electron spins, and the ferromagnetic state becomes more stable.

Using our values for ΔE_{stab} together with the local magnetic moments μ, it is possible to produce an estimate

TABLE II. Calculated lattice constants and binding energies compared with experiment.

Oxide	Lattice constant (Å) Calc.	Expt. (Ref. 31)	Binding energy (eV) Calc.	Expt. (Ref. 63)
MnO (AF_2)	4.5260	4.4448	6.2	9.5
NiO (AF_2)	4.2638	4.1684	6.2	9.5
MnO (ferro)	4.5239			
NiO (ferro)	4.2646			
MnO (AF_1)	4.5272			
NiO (AF_1)	4.2699			

TABLE III. Calculated spin magnetic moments $m_s(\mu_B)$ for the AF_2 state compared with experimental values.

		$m_s(\mu_B)$	
Oxide	Calc.	Expt.
MnO	4.923	4.58 (Ref. 64), 4.79 (Ref. 65)
NiO	1.924	1.64 (Ref. 66), 1.77 (Ref. 65), 1.90 (Ref. 64)

TABLE IV. Comparison of ferromagnetic state energies (eV/cell) at the calculated AF_2 lattice constant ($\sigma = 2S_z$ / cell).

MnO		NiO	
State	ΔE	State	ΔE
$t_{2g}^3 e_g^2(\sigma = 5)$	0.0	$t_{2g}^6 e_g^2(\sigma = 2)$	0.0
$t_{2g}^5(\sigma = 1)$	+10.69	closed shell	+11.31
$t_{2g}^4 e_g^1(\sigma = 3)$	+11.43	$t_{2g}^6 e_g^2(\sigma = 0)$	+11.86
closed shell	+12.79		

for the ratio of the Néel temperatures of the two systems. The UHF wave function is an eigenfunction of S_z but not of S^2, and thus most closely corresponds to an Ising model of the spin. Within mean-field theory the transition temperature of the Ising model is[33]

$$T_N = \frac{2z|J|S(S+1)}{3k_B},$$

where S is the total spin moment, k_B is the Boltzmann constant, and z is the number of second-nearest-neighbor metal ions which are involved in the superexchange interaction. In the Ising model ΔE_{stab} is $2S^2|J|z$. Hence

$$T_N \propto \frac{\Delta E_{stab}}{k_B}(1+S^{-1}).$$

The experimental ratio $T_N(\text{NiO})/T_N(\text{MnO})$ of 4.52 (Table V) compared favorably with our calculated ratio of 4.17. It is interesting to note that, assuming a proportionality constant of $\frac{4}{3}$, direct estimates of T_N are in fairly close agreement with experiment.

The observed ground-state spin arrangement of successively antiparallel ferromagnetic (111) planes gives rise to a magnetostriction effect within the crystal. This takes the form of a rhombohedral contraction normal to the ferromagnetic planes; at low temperature the crystal axes are inclined at 0.62° (MnO) and 0.1° (NiO) from the ideal cubic directions.[34,35] The distortion increases with increasing temperature.

Figures 1(a) and 1(b) show the calculated variation of the total energy of the AF_2 state as a function of a volume-conserving rhombohedral distortion. Analogous curves for the ferromagnetic state are also shown. For both materials, the shift in the minimum for the AF_2 state corresponds to a contraction along the [111] axis in

TABLE V. Calculated antiferromagnetic stabilization energies relative to the ferromagnetic state (eV/double cell) at the calculated AF_2 lattice constant. Calculated and experimental Néel temperatures (K).

Oxide	$\Delta E_{stab}(AF_2)$	$\Delta E_{stab}(AF_1)$	T_N (Estimated)	T_N (Expt.)
MnO	−0.0115	+0.0004	94	116
NiO	−0.0331	+0.0119	392	525
			ratio: 4.17	ratio: 4.53

TABLE VI. Deviations from ideal cubic (90°) angles in the AF_2 state due to exchange magnetostriction.

Oxide	Calc.	Expt.
MnO	90.47°	90.62° (Ref. 34)
NiO	90.075°	90.1° (Ref. 35)

accordance with experiment. As one would expect, the calculation produced no distortion from cubic symmetry in the ferromagnetic state. Furthermore, the calculated equilibrium deviations from the ideal cubic angles in the AF_2 case are in good agreement with experiment (Table VI).

B. Electronic structure

We first consider the Mulliken population analyses presented in Table VII. The charge transfer of around $1.9e$ indicates that both compounds can be qualitatively described as classical ionic oxides. This is supported further by the $3d$ populations and atomic spin moments, given in Table VIII, which are characteristic of $t_{2g}^3 e_g^2$ (Mn) and $t_{2g}^6 e_g^2$ (Ni) configurations of the free +2 cations in an octahedral environment. Electron-density difference maps [Figs. 2(a) and 2(b)] were obtained by subtracting the spherical atomic charge distributions (derived from the free ion solutions) away from the bulk density. Both charge densities refer to the basis set optimized in the solid. The figures, which show the basal (100) plane of the unit cell, demonstrate significant contractions of the atomic orbitals of both anions and cations in the solid relative to the free ions. This contraction is presumably due to short-range exchange repulsions and, for the anion, to the confining effect of the Madelung potential. This qualitative picture may explain the success of ionic model calculations for the lattice and defect properties of the transition-metal monoxides.[36-38] There is clear evidence for the preferential occupation of the t_{2g} levels in NiO in the nonspherical symmetry of both the electron-density difference and spin-density maps shown in Figs. 2(b) and 2(d), respectively, as observed experimentally.[39] The corresponding maps for MnO, Figs. 2(a) and 2(c), show equally clearly the spherical d^5 ($t_{2g}^3 e_g^2$) electron configuration of Mn^{2+}.

The calculated band structures for the ferromagnetic and AF_2 states are given in Fig. 3. Selected directions and special points in the Brillouin zones, which are illustrated in Fig. 4, follow the notation given by Bradley and Cracknell[40] and Slater[41] for the ferromagnetic (fcc) and the AF_2 (rhombohedral) cases, respectively. The calculated band structures are broadly similar for each magnetic state. In NiO the valence bands are centered at −0.18 hartree with a bandwidth of 0.36 hartree and a band gap of 0.5 hartree. The projected density of states (DOS) are shown in Fig. 5. The lower and upper valence bands have predominantly Ni d and O p character, respectively and hybridize strongly in the center of the band. The conduction band includes contributions from both Ni and O orbitals, although the lower edge is largely
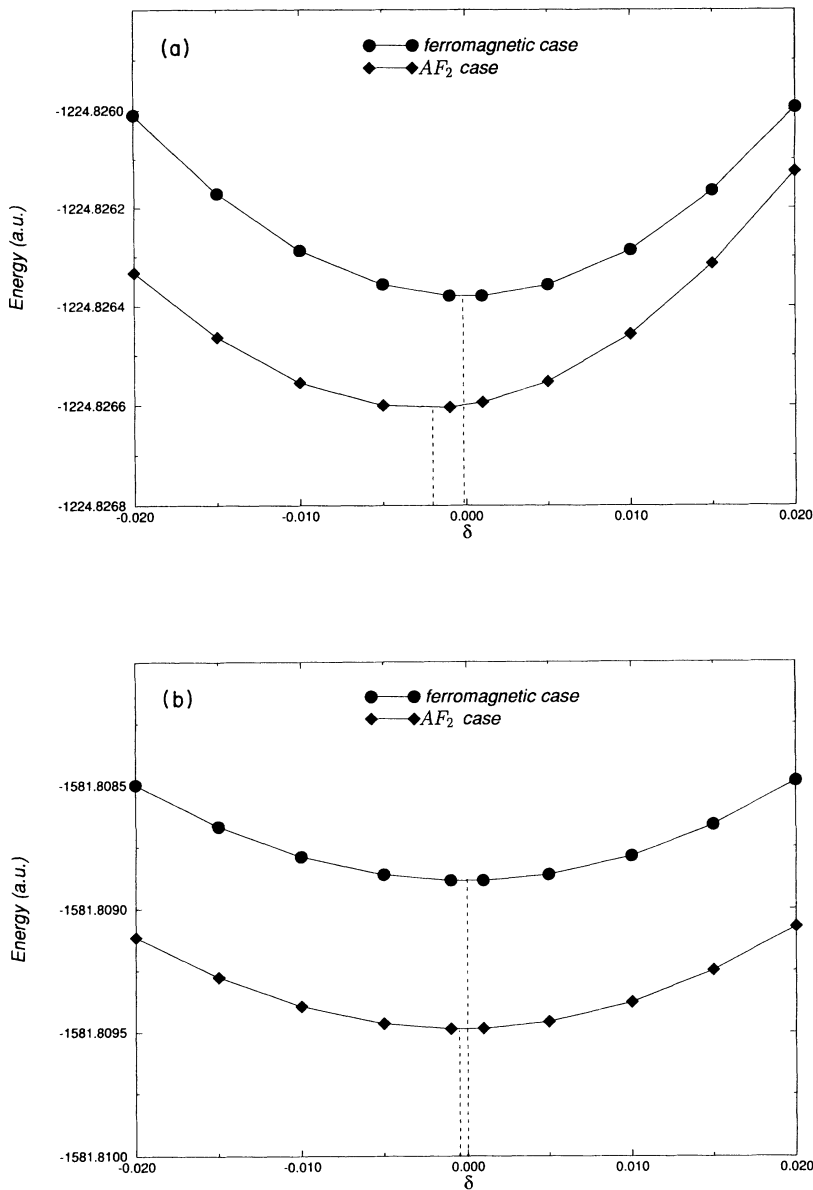
AB INITIO STUDY OF MnO AND NiO

FIG. 1. Energetic response of (a) MnO and (b) NiO to an elastic C_{44} distortion. The nonzero components of the symmetric Lagrangian elastic tensor are $\delta/2$.

TABLE VII. Distribution of charge among atomic orbitals in the AF_2 state following Mulliken population analysis.

Oxide	Atom	Mulliken population orbital						
		$1s$	$2sp$	$3sp$	$4sp$	$5sp$	$3d$	$4d$
MnO	Mn	2.000	8.082	2.164	4.293	1.487	4.502	0.611
							$t_{2g}2.652$	$t_{2g}0.375$
							$e_g1.85$	$e_g0.236$
	O	1.997	2.640	2.628	2.602			
NiO	Ni	2.000	8.147	2.403	4.262	1.222	6.659	1.430
							$t_{2g}4.911$	$t_{2g}1.08$
							$e_g1.748$	$e_g0.35$
	O	1.997	2.647	2.664	2.566			

β-spin e_g. In the present work α and β denote majority and minority spins, respectively. The picture in MnO is similar but the now unoccupied β-spin t_{2g} band is relocated to the lower edge of the conduction band. The calculations thus indicate holes that are predominantly O p in character, in contrast to the conventional Mott-Hubbard view of MnO and NiO, which predicts mainly metal $3d$ character in the upper valence bands.[42,43] The recent SIC-LSD calculations of Svane and Gunnarsson[11] are in broad agreement with these findings. Furthermore, oxygen K-edge x-ray-absorption data for lithium-doped NiO (Ref. 27) have suggested the presence of O p hole states in $Li_x Ni_{1-x}O$ for values of x in the range 0.05–0.5.

Some insight into the energy-level ordering of the d orbitals can be obtained from a single site model. Brandow[8,10] suggested that early band calculations of these materials had failed due to their treatment of the intra-atomic $3d$ interactions, and proposed that the d-d interaction term in the Hubbard Hamiltonian (U_H) be

TABLE VIII. Calculated Mulliken charges q, $3d$ orbital populations n_{3d}, and net atomic spins $\delta n_s(M)$ and $\delta n_s(O)$ for the three magnetic states.

Oxide	q	n_{3d}	$\delta n_s(M)$	$\delta n_s(O)$
MnO (AF_2)	1.864	5.122	4.924	0.000
NiO (AF_2)	1.875	8.090	1.923	0.000
MnO (AF_1)	1.867	5.108	4.925	0.030
NiO (AF_1)	1.879	8.085	1.934	0.024
MnO (ferro.)	1.862	5.126	4.920	0.081
NiO (ferro.)	1.880	8.097	1.931	0.069

parametrized by the set of three Kanamori[44] parameters U, U', and J. This proposal, essentially a model of the Hartree-Fock Hamiltonian, is prompted by the recognition that the self-exchange energy between electrons in the same localized d orbital is an order of magnitude greater than the exchange interaction between electrons in different d orbitals on the same site. U refers to the $3d$
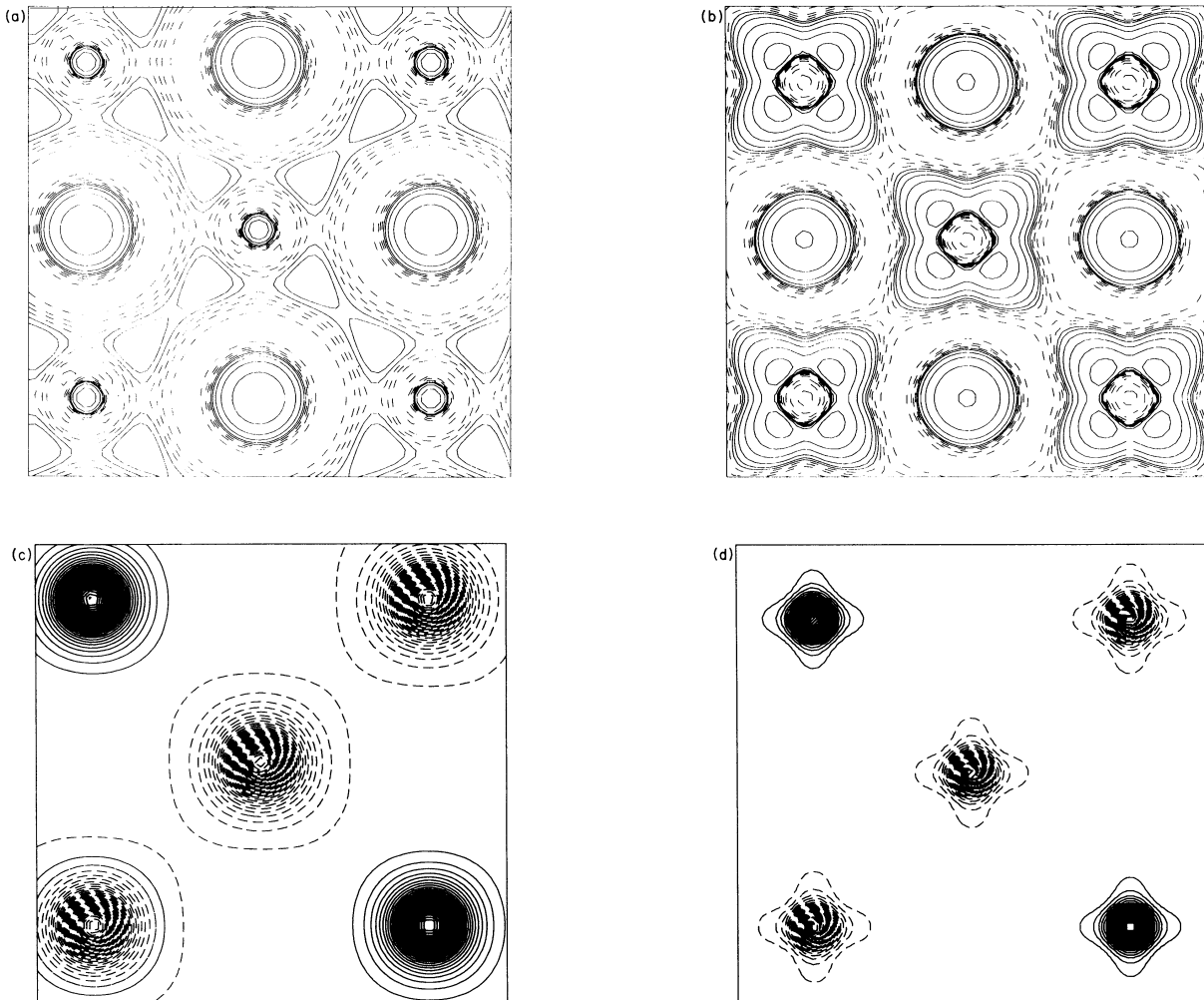

FIG. 2. Charge-density difference maps (bulk minus atom superposition) in the basal {100} plane for (a) MnO and (b) NiO and spin-density difference maps $(n_\alpha - n_\beta)$ for (c) MnO and (d) NiO. Continuous and dashed lines refer to positive and negative values, respectively.

self-interaction term, which is equivalent to the direct Coulomb repulsion between electrons in the same d orbital, U' to the on-site Coulomb repulsion between electrons in different d orbitals, and J to the on-site exchange interaction between different d orbitals (which only operates between electrons of the same spin). Note that U' and J are averaged over all possible pairs of orbitals involved in the interactions, and that after such averaging $U' = U - 2J$.

Consider first a high-spin d^8 Ni^{2+} ion in the octahedral field of the crystalline environment. The t_{2g} and e_g sub-bands are split through electrostatic crystal-field effects, with e_g higher in energy by Δ_{CF}. Intra-atomic interactions produce further shifts, the magnitudes of which can be deduced from a consideration of the ground-state electronic configuration $(\alpha\text{-}t_{2g})^3(\beta\text{-}t_{2g})^3(\alpha\text{-}e_g)^2$. Such considerations lead to the following splittings:

$$\Delta E_1 = E(\alpha\text{-}t_{2g}) - E(\alpha\text{-}e_g) = 2J - \Delta_{CF} ,$$

$$\Delta E_2 = E(\beta\text{-}t_{2g}) - E(\alpha\text{-}t_{2g}) = 2J ,$$

$$\Delta E_3 = E(\beta\text{-}e_g) - E(\beta\text{-}t_{2g}) = U - 3J + \Delta_{CF} .$$
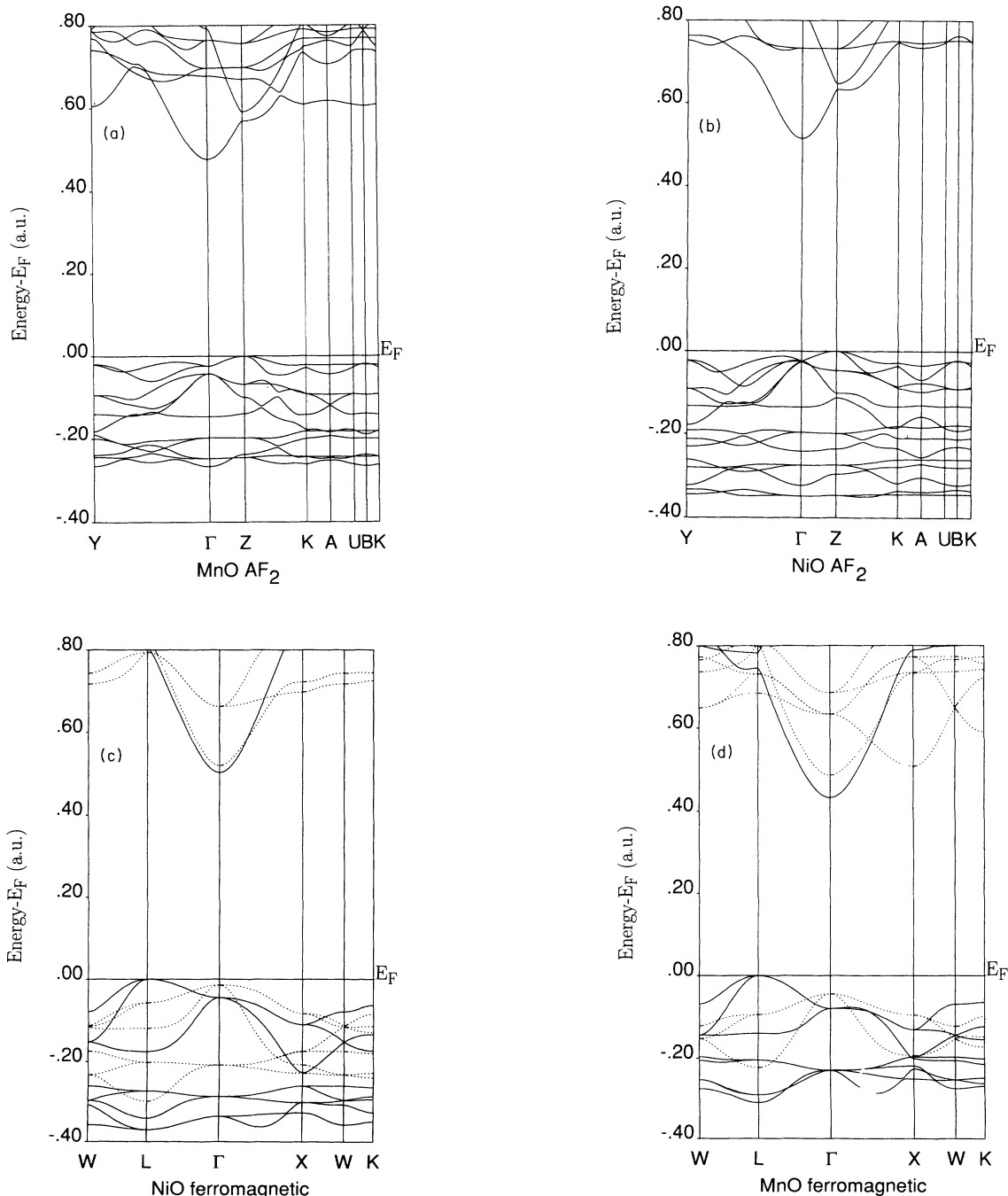
FIG. 3. $E(k)$ curves along high-symmetry directions for the AF_2 and ferromagnetic states of MnO and NiO. Minority-spin electron states are indicated with a dashed line for the ferromagnetic case.
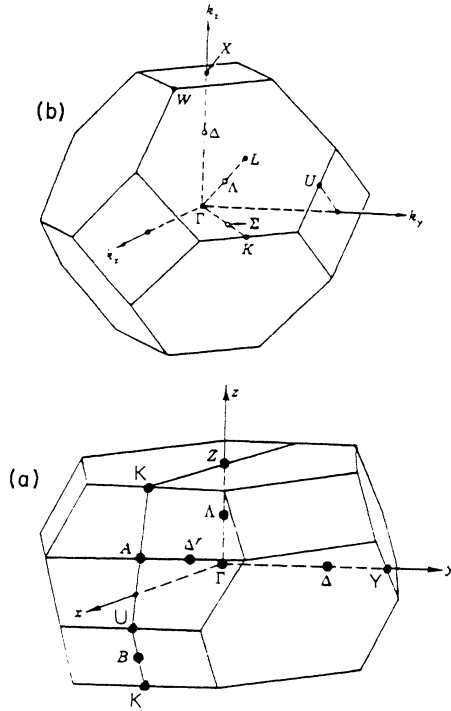
FIG. 4. First Brillouin zones of (a) AF_2 and (b) ferromagnetic unit cells.

The corresponding energy-level diagram is given in Fig. 6(a). We have evaluated the necessary integrals at the experimental lattice parameter using Ni d radial functions optimized in the bulk, yielding values of 1.026, 0.037, and 0.012 hartree for U, J, and Δ_{CF}, respectively. The predicted splittings are therefore 0.062, 0.074, and 0.927 hartree for ΔE_1, ΔE_2, and ΔE_3, respectively, to be compared with 0.051, 0.078, and 0.867 hartree found from the calculated band structure at the Γ point. The discrepancies between these two sets of results are well within the calculated bandwidths, the latter being due to intersite interactions (covalency). The α-spin e_g states are at a lower energy than the α-spin t_{2g} states, in disagreement with simple crystal-field rules,[45] because of intra-atomic interactions. This splitting persists even if measured from the centroid of the bands [Fig. 5(d)]. These interactions introduce an energy band between the valence and conduction bands of order U, and the insulating nature of NiO is thus primarily the result of on-site Coulombic repulsion, which is sufficient to open a larger gap. Furthermore, this band-splitting pattern should apply to all possible spin configurations, since U is very much larger than J, so that we expect the insulating properties will persist above T_N as experimentally observed. It is worth noting that Brandow[9] had deduced the values 0.213, 0.026, and 0.040 hartree for U, J, and Δ_{CF}, respectively, from spectroscopic data, giving rise to a much smaller band gap than that found in the present work. However, it should be remembered that differences in Hartree-Fock eigenvalues do not strictly

correspond to excitation energies even within a frozen orbital picture; the experimental data will also be affected by correlation, and probably more importantly, relaxation effects which will considerably lower the observed excitation energies. It can therefore safely be concluded that the Hartree-Fock band gap will be a considerable overestimate of the observed optical gap, and that is it not appropriate to interpret spectroscopic data in terms of Hartree-Fock eigenvalues. Some success has been achieved through applying ΔSCF and configuration-interaction techniques to compute excitation energies. Janssen and Nieuwpoort[22] estimated the correlation correction in charge-transfer excitation energies to be 1–2 eV in $[NiO_6]^{10-}$ clusters, and Massidda, Posternak, and Baldereschi[46] used a screened Coulomb interaction to estimate correlation effects on the band gap in $CaCuO_2$ to be ~ 5 eV. The reason for the failure of the LSDA to predict a sufficiently large gap[7,47–49] is because the value of U obtained from a local homogeneous electron-gas approximation is very much smaller than that evaluated directly.[9,50]

A similar analysis of the band structure of MnO yields

$$\Delta E_1 = E(\alpha\text{-}e_g) - E(\alpha\text{-}t_{2g}) = \Delta_{CF} \ ,$$

$$\Delta E_2 = E(\beta\text{-}t_{2g}) - E(\alpha\text{-}e_g) = U + 4J - \Delta_{CF} \ ,$$

$$\Delta E_3 = E(\beta\text{-}e_g) - E(\beta\text{-}t_{2g}) = \Delta_{CF} \ ,$$

and the resulting energy-level diagram is shown in Fig. 6(b). We have again evaluated the necessary integrals at the experimental lattice parameter using Mn d-orbital radial functions optimized in the bulk, resulting in 0.861, 0.031, and 0.017 hartree for U, J, and Δ_{CF}, respectively. The predicted splittings are therefore 0.017, 0.968, and 0.017 hartree for ΔE_1, ΔE_2, and ΔE_3, respectively, to be compared with -0.001, 0.861, and 0.054 hartree found from the calculated band structure at the Γ point. The discrepancies between these two sets of results are again within the calculated bandwidths. A surprising feature of the MnO density of states is the amount of $\alpha\text{-}e_g$ density which lies below the $\alpha\text{-}t_{2g}$ band. This is primarily due to metal-oxygen covalent σ bonding which stabilizes the occupied e_g orbitals relative to the t_{2g}. Even at Γ, where there is no such mixing, the interatomic terms are such that e_g lies at slightly lower energy. Overall, the splitting is small compared to the subband widths, and it is not clear that it would persist if measured from the band centroids [Fig. 5(a)].

C. Elastic properties

The elastic constants and phonon dispersion curves of ionic and partially ionic compounds have usually been calculated using classical approaches based on semi-empirical formulas of the Born type.[51] The central-force potentials used to represent the ground-state energy of the solid as a function of the nuclear positions in these methods require a set of empirical parameters to specify their functional form. These are usually determined by fitting to available experimental data such as binding en-
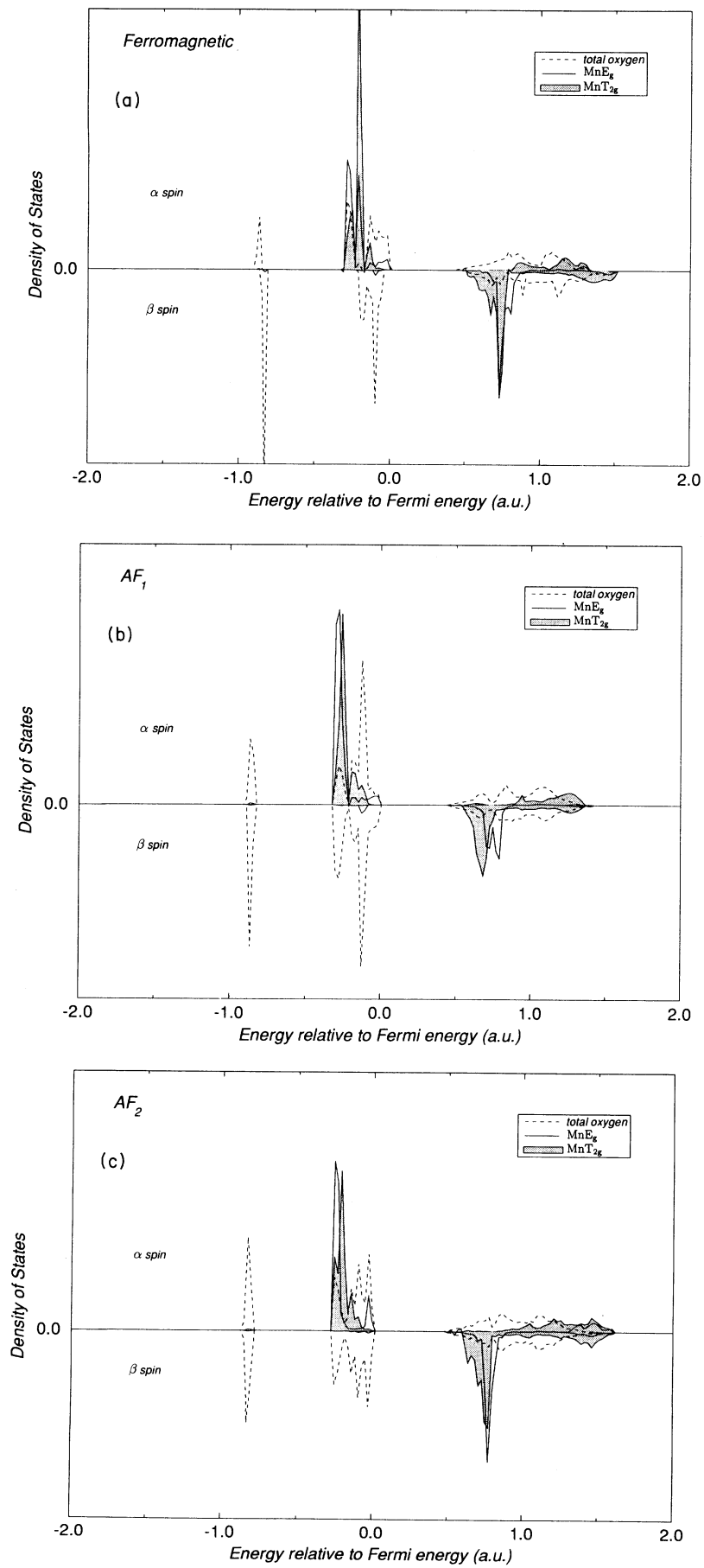
FIG. 5. Band-projected density of states showing valence and lower conduction bands of (a)–(c) MnO and (d)–(f) NiO in ferromagnetic, AF_1, and AF_2 states.
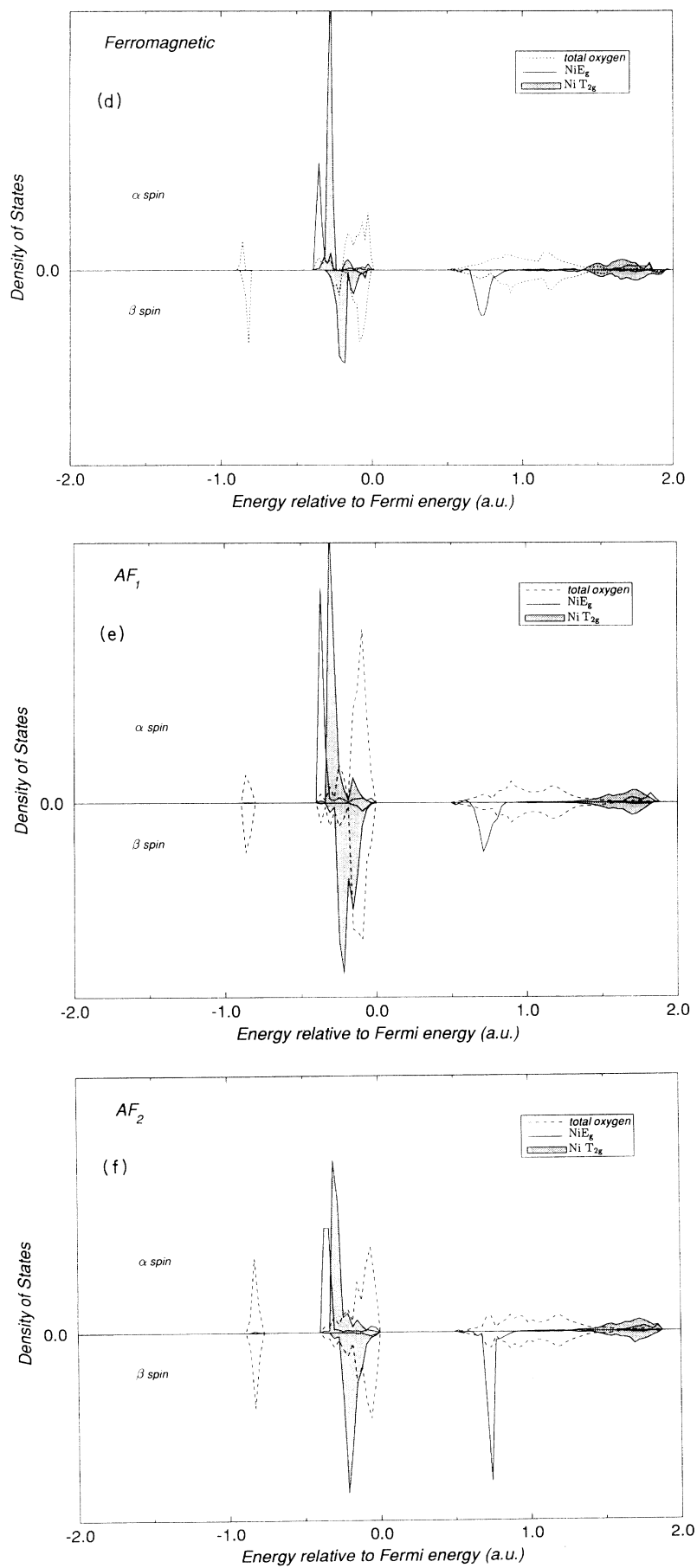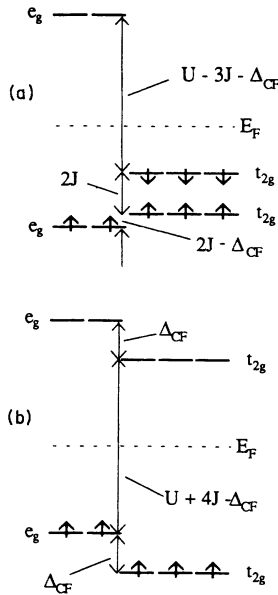
FIG. 5. (*Continued*).

FIG. 6. Splitting of the $3d$ subbands in (a) NiO and (b) MnO following the scheme presented in the text.

ergy, lattice parameter, and dielectric constants. The Hartree-Fock approach, as implemented in CRYSTAL, allows a parameter-free *ab initio* determination of such properties even for materials where experimental data is unavailable, e.g., Refs. 17 and 52. Here calculations of the elastic constants and phonon frequencies of MnO and NiO are reported.

1. Elastic constants

The static elastic constants C_{ij} are second derivatives of the energy density with respect to strain components,

$$C_{ij} = \frac{1}{V} \frac{\partial^2 E}{\partial s_i \partial s_j} ,$$

where V is the volume of the cell and E is the energy per cell. The total energies of NiO and MnO were calculated as a function of elastic strains of up to 2%, then fourth-order polynomial fits of the resulting data were employed to obtain the appropriate second derivatives at the energy minimum.

By simple variation of the lattice constant of the cubic unit cell, an isotropic deformation of the crystal structure was obtained, yielding both the equilibrium geometry and the bulk elastic modulus B. The three independent components of the elastic tensor were then derived as follows. C_{11} was given directly by deforming one of the three edges of the cubic unit cell. C_{12} was calculated indirectly, via the linear combination C_{11}-C_{12}, from a volume-conserving strain involving the contraction of two edges and the stretching of the other by twice as much. The shear constant C_{44} resulted from the application of a volume-conserving rhombohedral strain along the $\langle 111 \rangle$ direction. As an internal consistency check one can compute the bulk modulus from the formula $B = (C_{11} + 2C_{12})/3$. Strains of 2% correspond to tetrago-

nal distortions of the cell sides by 0.08–0.09 Å in the C_{11} and C_{11}-C_{12} cases, and deviations of the cell angles from 60° of about 1.3° in the rhombohedral case (C_{44}). Since all the atoms are at centrosymmetric sites no internal positional relaxations are possible.

The calculated constants for both ferromagnetic and AF_2 magnetic states are shown in Table IX, together with experimental data from a number of sources. Our calculations ignore any lattice-vibrational contributions to the free energy and thus should be compared to measurements extrapolated to the athermal limit. Unfortunately the wide variation in the published experimental data for NiO (Refs. 53–55) makes detailed comparison difficult. For MnO room-temperature measurements using ultrasonic techniques are broadly in agreement with each other,[54,56–58] although attempts to measure the constants below the antiferromagnetic ordering temperature have met with mixed success. In particular the C_{44} shear constant softens dramatically on approaching T_N, and below T_N acoustic attenuation appears to be too strong to obtain an accurate measurement.[58] In many instances, sharp discontinuities in elastic constants have been observed on passing through the Néel temperature of antiferromagnetic materials,[53] so any attempt to extrapolate from linear curves in the paramagnetic region to absolute zero is likely to produce large errors. Hence the value of C_{44} in the athermal limit is unclear. The theoretical predictions for the other constants, Table IX(a), are seen to be in reasonable agreement with experiment, errors ranging from +3 to 28%. The value of C_{44} for the AF_2 state is around 5% less than that calculated for the ferromagnetic state, whereas the other constants are insensitive to the magnetic order.

For comparative purposes the elastic constants of CaO, MnO, and NiO were also calculated using a semiempirical classical technique. A two-body interatomic potential shell model was employed within an ionic model framework. The consistent set of potentials and shell model parameters used is due to Stoneham and Sangster.[59] As is well known, two-body forces cannot account for the experimentally observed Cauchy violation. Nevertheless there are clear trends in the calculated values along the series Ca to Ni and, bearing in mind the limitations of the two-body model, the values support the *ab initio* calculations.

2. Phonon frequencies

The phonon spectra of both materials have been determined experimentally.[60,61] We have calculated the phonon frequencies at the Γ and L points in the first Brillouin zone using the frozen-phonon approximation; we assume that the acoustic and optical modes do not couple. Ionic displacements of 0.025 Å were used, and energy curves fitted with fourth-order polynomials. Coulomb terms were summed using the Ewald convention and thus no macroscopic fields are generated; therefore the Γ-point distortion corresponds to the transverse-optic (TO) mode. The calculated values, reported in Table X, tend to be somewhat higher than experiment. This is con-

TABLE IX. (a) Calculated elastic constant and bulk modulus data for MnO compared with experimental data at various temperatures. (b) Calculated elastic constant and bulk modulus data for NiO compared with experimental data at various temperatures. (c) Elastic constants calculated using a semiempirical two-body potential model for CaO, MnO, and NiO. An *ab initio* Hartree-Fock study of CaO gave a value of 128 GPa for the bulk modulus (Ref. 28).

(a)

			Expt.			MnO elastic constants (GPa) Calc.	
T (K)	C_{ij}	Ref. 57	Ref. 58	Ref. 54	Ref. 56	Ferro	AF_2
0	C_{11}		~231			281	
	C_{11}-C_{12}	123.6	~119			166	
	C_{12}		~112			115	
	C_{44}					96	90.6
	B		~152			170	169
50	C_{11}		230.5				
	C_{11}-C_{12}	123.4	119.5				
	C_{12}		111				
	C_{44}						
	B		150.8				
116 (T_N)	C_{11}		231.4				
	C_{11}-C_{12}	124.6	120.9				
	C_{12}		110.5				
	C_{44}	~40	~48				
	B		149.3				
298	C_{11}			222	223		
	C_{11}-C_{12}	116		109.9	103		
	C_{12}			112.1	120		
	C_{44}	77		78	78.3	79	
	B			148.6	154.3		

(b)

NiO elastic constants (GPa)

				Expt.				Calc.	
T (K)	C_{ij}	Ref. 53	Ref. 54	Ref. 67	Ref. 55	Ref. 68	Ref. 69	Ferro.	AF_2
0	C_{11}	211						399	
	C_{11}-C_{12}	90						272	
	C_{12}	121						127	
	C_{44}	109						121	115
	B	145						215	214
298	C_{11}	224	271		344.6				
	C_{11}-C_{12}	132	145		203.3				
	C_{12}	97	125		141.3				
	C_{44}	110	105		40				
	B	137	173	189	205	190	199		

(c)

Elastic constants (GPa)

	CaO	MnO	NiO
C_{11}	217	272	450
C_{12}	94	128	163
C_{44}	94	128	163
B	134	175	258

AB INITIO STUDY OF MnO AND NiO

TABLE X. Γ-point and L-point phonon frequencies (THz). [Expt. (Refs. 60 and 61)].

	Γ point				L point					
	TO		LA		TA		LO		TO	
Oxide	Expt.	Calc.	Expt.	Calc.	Expt.	Calc.	Expt.	Calc.	Expt.	Calc.
MnO	7.9	9.5	9.0	10.91	4.8	5.70	15.6	17.88	8.0	9.46
NiO	11.6	11.8	10.0	11.28	6.2	6.24	16.3	17.81	10.4	11.32

sistent with previous experience of molecular and periodic Hartree-Fock calculations which tend to overestimate vibrational frequencies. A posteriori density-functional correlation corrections soften all of the lattice vibrations at the Γ, X, and L points in MgO.[62] The neglect of coupling between the L-point modes may also be a source of error.

IV. CONCLUSIONS

The Hartree-Fock method generates a qualitatively correct ground-state electronic structure in NiO and MnO in which the wide-band-gap insulating character of these materials is seen to be a result of the large on-site Coulomb interactions. The materials are correctly predicted to be antiferromagnetic with AF_2 structure. The relative energy differences between various magnetic structures are consistent with the ratio of the Néel temperatures. The structural, elastic, and vibrational properties are in reasonable agreement with available experimental data.

ACKNOWLEDGMENTS

[1]D. Adler, in Solid State Physics, edited by H. Ehrenreich and D. Turnbull (Academic, New York, 1968), Vol. 21, p. 1.

[2]A. B. Kunz, J. Phys. C 14, L455 (1981).

[3]C. Kittel, Introduction to Solid-State Physics (Wiley, New York, 1986).

[4]J. Zaanen, G. A. Sawatzky, and J. W. Allen, Phys. Rev. Lett. 55, 418 (1984).

[5]J. B. Torrance, P. Lacorre, C. Asavaroengchai, and R. M. Metzger, Physica C 182, 351 (1991).

[6]K. Schwartz, in Basic Properties of Binary Oxides, edited by A. Dominguez Rodriguez, J. Castaing, and R. Marquez (Servicio de Publicaciones de la Universidad de Sevilla, Seville, 1984), p. 43.

[7]K. Terakura, A. R. Williams, T. Oguchi, and J. Kübler, Phys. Rev. B 30, 4734 (1984).

[8]B. H. Brandow, Adv. Phys. 24, 651 (1977).

[9]B. Brandow, in Narrow-Band Phenomena—Influence of Electrons with Both Band and Localised Character, edited by J. C. Fuggle, G. A. Sawatzky, and J. W. Allen (Plenum, New York, 1988), p. 97.

[10]B. Brandow, J. Alloys Compounds 181, 377 (1992).

[11]A. Svane and O. Gunnarsson, Phys. Rev. Lett. 65, 1148 (1990).

[12]V. I. Anisimov, J. Zaanen, and O. K. Andersen, Phys. Rev. B 44, 943 (1991).

[13]C. Pisani, R. Dovesi, and C. Roetti, Hartree-Fock Ab Initio Treatment of Crystalline Systems (Springer-Verlag, Berlin, 1988).

[14]R. Dovesi, V. R. Saunders, and C. Roetti, CRYSTAL92, User Manual (Università di Torino and SERC Daresbury Laboratory, 1992)

[15]J. A. Pople and R. K. Nesbet, J. Chem. Phys. 22, 571 (1954).

[16]R. Dovesi, Solid State Commun. 54, 183 (1985).

[17]R. Dovesi, C. Roetti, C. Freyria-Fava, M. Prencipe, and V. R. Saunders, Chem. Phys. 156, 11 (1991).

[18]M. Causà, R. Dovesi, C. Pisani, and C. Roetti, Phys. Rev. B 33, 1388 (1986); 34, 2939 (1986).

[19]M. Causà, R. Dovesi, C. Roetti, and V. R. Saunders, Chem.

Phys. Lett. 140, 20 (1987).

[20]L. Salasco, R. Dovesi, R. Orlando, M. Causà, and V. R. Saunders, Mol. Phys. 72, 267 (1991).

[21]W. C. Mackrodt, N. M. Harrison, V. R. Saunders, N. L. Allan, M. D. Towler, E. Aprà, and R. Dovesi, Philos. Mag. A 68, 653 (1993).

[22]G. J. M. Janssen and W. C. Nieuwpoort, Phys. Rev. B 38, 3449 (1988).

[23]A. Fujimori, F. Minami, and S. Sugano, Phys. Rev. B 29, 5225 (1984).

[24]A. Fujimori and F. Minami, Phys. Rev. B 30, 957 (1984).

[25]G. A. Sawatzky and J. W. Allen, Phys. Rev. Lett. 53, 2239 (1984).

[26]S. Hüfner and T. Riesterer, Phys. Rev. B 33, 7267 (1986).

[27]P. Kuiper, G. Kruizinga, J. Ghijsen, G. A. Sawatzky, and H. Verweij, Phys. Rev. Lett. 62, 221 (1989).

[28]R. Dovesi, C. Roetti, C. Freyria-Fava, E. Aprà, V. R. Saunders, and N. M. Harrison, Philos. Trans. R. Soc. London Ser. A 341, 203 (1992).

[29]R. Dovesi, M. Causà, R. Orlando, C. Roetti, and V. R. Saunders, J. Chem. Phys. 92, 7402 (1990).

[30]H. J. Monkhorst and J. D. Pack, Phys. Rev. B 13, 5188 (1976).

[31]R. W. G. Wyckoff, Crystal Structures (Interscience, New York, 1964).

[32]E. Aprà, Ph.D. thesis, Università di Torino, 1993.

[33]J. H. van Vleck, J. Chem. Phys. 9, 85 (1941).

[34]H. Shaked, J. Faber, and R. L. Hittermann, Phys. Rev. B 38, 11 901 (1988).

[35]G. A. Slack, J. Appl. Phys. 31, 1571 (1960).

[36]C. R. A. Catlow, B. E. F. Fender, and D. G. Muxworthy, J. Phys. (Paris) C 7, 67 (1975).

[37]M. J. L. Sangster and A. M. Stoneham, Philos. Mag. B 43, 609 (1980).

[38]W. C. Mackrodt, Solid State Ionics 12, 175 (1984).

[39]S. Sasaki, K. Fujino, and Y. Takeuchi, Proc. Jpn. Acad. B 55, 43 (1979).

[40]C. J. Bradley and A. P. Cracknell, *The Mathematical Theory of Symmetry in Solids: Representation Theory for Point Groups and Space Groups* (Clarendon, Oxford, 1970).

[41]J. C. Slater, *Quantum Theory of Molecules and Solids, Vol. II: Symmetry and Energy Bands in Crystals* (McGraw-Hill, New York, 1965).

[42]P. A. Cox, *The Transition Metal Oxides* (Oxford University Press, Oxford, 1992).

[43]K. Terakura, A. R. Williams, T. Oguchi, and J. Kübler, Phys. Rev. Lett. **52**, 1830 (1984).

[44]J. Kanamori, Prog. Theor. Phys. **30**, 275 (1963).

[45]F. A. Cotton and G. Wilkinson, *Advanced Inorganic Chemistry*, 2nd ed. (Wiley, New York, 1966), p. 660.

[46]S. Massidda, M. Posternak, and A. Baldereschi, Phys. Rev. B **46**, 11 705 (1992).

[47]O. K. Andersen, H. L. Skriver, H. Nohl, and B. Johannsson, Pure Appl. Chem. **52**, 93 (1979).

[48]T. Oguchi, K. Terakura, and A. R. Williams, Phys. Rev. B **28**, 6443 (1983).

[49]J. Kübler and A. R. Williams, J. Magn. Magn. Mater. **54-57**, 603 (1986).

[50]L. Severin, M. S. S. Brooks, and B. Johannsson, Phys. Rev. Lett. **71**, 3214 (1993).

[51]C. R. A. Catlow, M. Dixon, and W. C. Mackrodt, in *Computer Simulation of Solids*, edited by C. R. A. Catlow and W. C. Mackrodt (Springer-Verlag, Berlin, 1982), p. 130.

[52]M. Catti, A. Pavese, R. Dovesi, C. Roetti, and M. Causà, Phys. Rev. B **44**, 3509 (1991).

[53]P. d. V. DuPlessis, S. J. Van Tonder, and L. Alberts, J. Phys. C **4**, 1983 (1971).

[54]N. Uchida and A. Saito, J. Acoust. Soc. Am. **51**, 1602 (1972).

[55]J. Wang, E. S. Fisher, and M. H. Manghnzmi, Chin. Phys. Lett. **8**, 153 (1991).

[56]D. W. Oliver, J. Appl. Phys. **40**, 893 (1969).

[57]S. B. Palmer and A. Waintal, Solid State Commun. **34**, 663 (1980).

[58]D. Seino, J. Magn. Magn. Mater. **28**, 55 (1982).

[59]A. M. Stoneham and M. J. L. Sangster, Philos. Mag. B **52**, 717 (1985).

[60]V. Wagner, W. Reichhardt, and W. Kress, in *Proceedings of the Conference on Neutron Scattering, Gatlinburg*, edited by R. M. Moon (NTIS, Springfield, VA, 1976), Vol. 1, p. 175.

[61]W. Reichardt, V. Wagner, and W. Kress, J. Phys. C **8**, 3955 (1975).

[62]M. I. McCarthy and N. M. Harrison, Phys. Rev. B **49**, 8574 (1994).

[63]I. Barin, *Thermochemical Data of Pure Substances* (VCH, Cambridge, 1989).

[64]A. K. Cheetham and D. A. O. Hope, Phys. Rev. B **27**, 6964 (1983).

[65]B. E. F. Fender, A. J. Jacobson, and F. A. Wedgewood, J. Chem. Phys. **48**, 990 (1968).

[66]H. A. Alperin, J. Phys. Soc. Jpn. Suppl. B **17**, 12 (1962).

[67]I. Wakabayashi, H. Kobayashi, H. Nagasaki, and S. Minomura, J. Phys. Soc. Jpn. **25**, 227 (1968).

[68]M. R. Notis, R. M. Spriggs, and W. C. Hahn, J. Geophys. Rev. **76**, 7052 (1971).

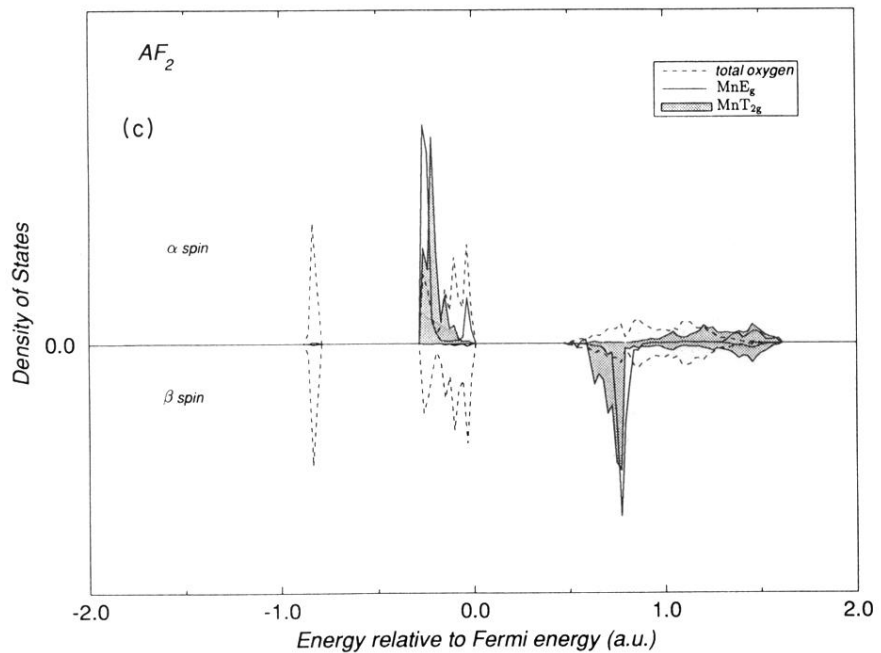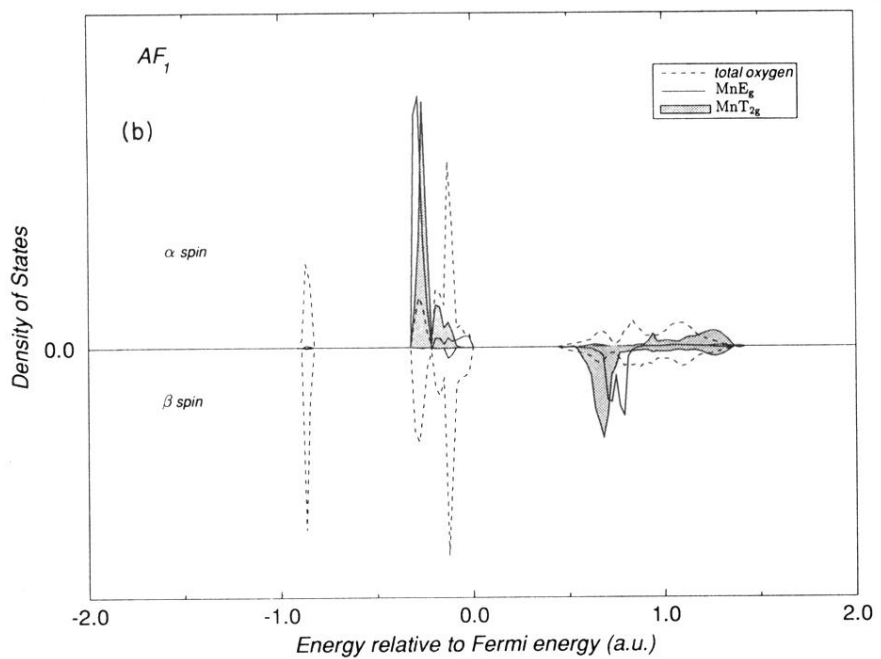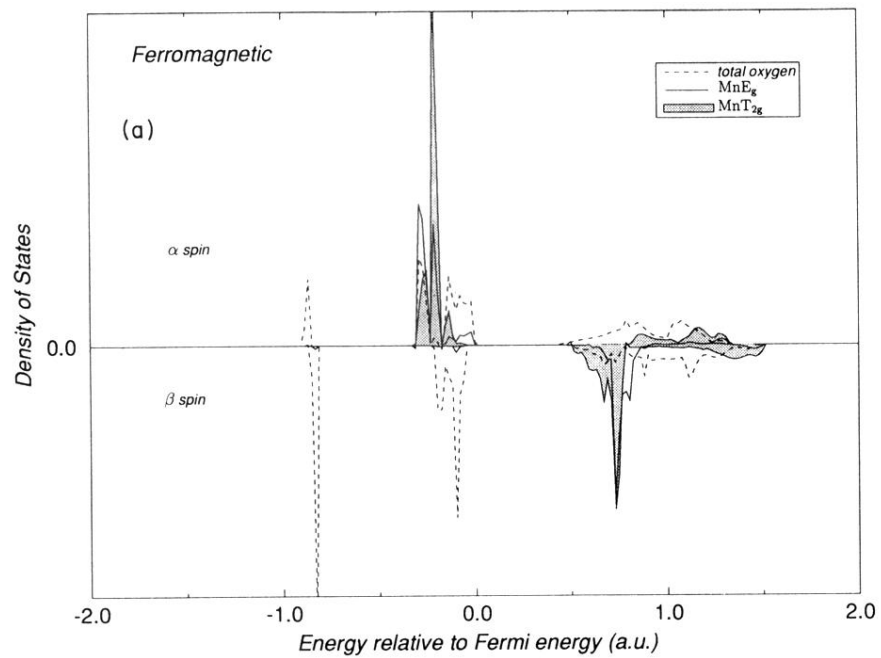[69]R. L. Clenenden and H. G. Drickamer, J. Chem. Phys. **44**, 4223 (1966).

FIG. 5. Band-projected density of states showing valence and lower conduction bands of (a)–(c) MnO and (d)–(f) NiO in ferromagnetic, AF_1, and AF_2 states.
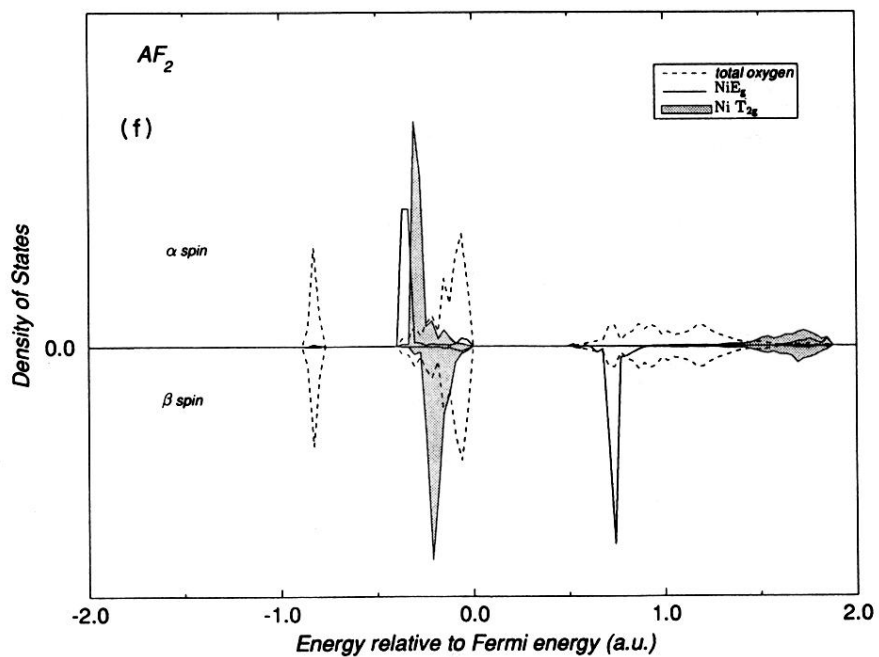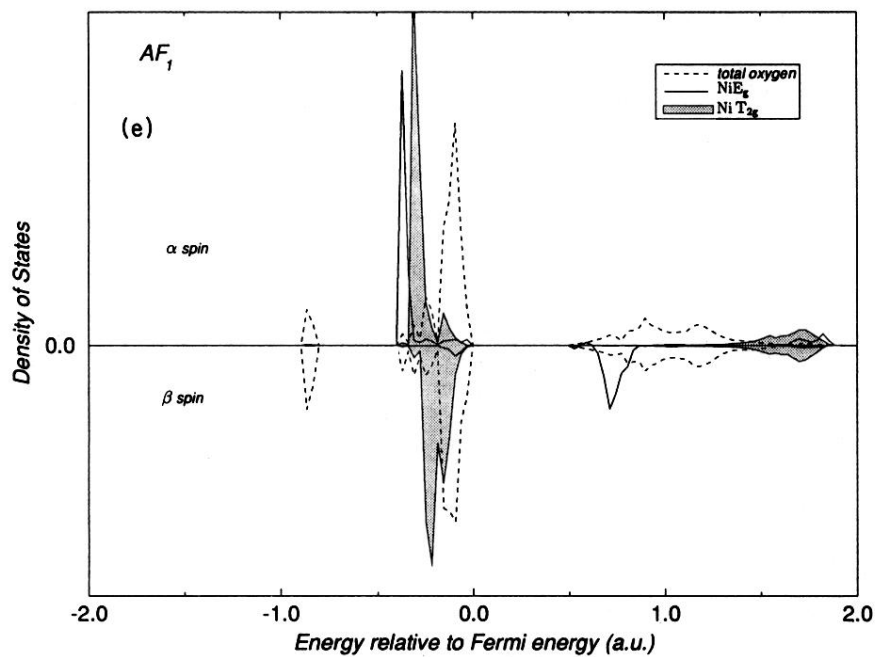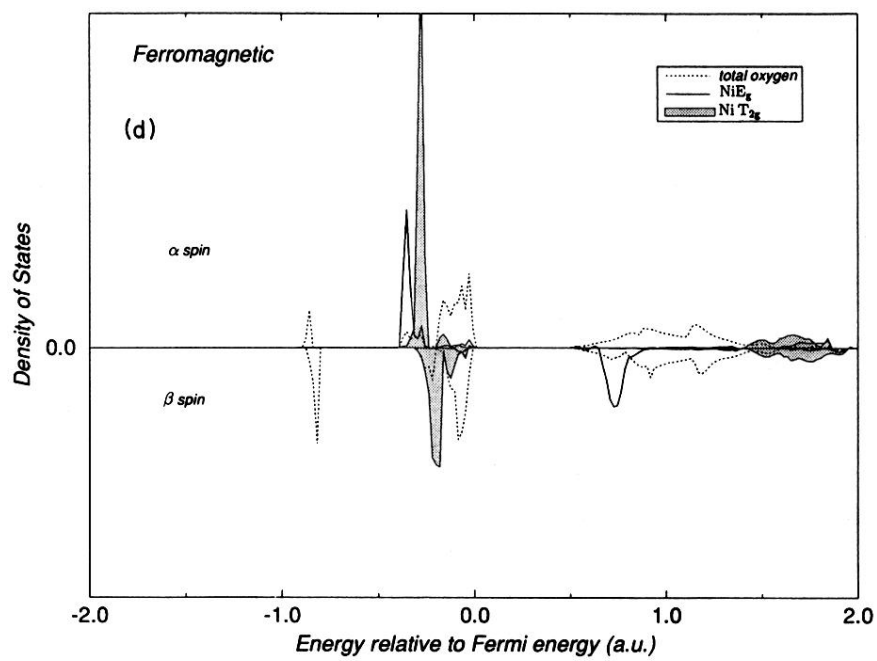
FIG. 5. (*Continued*).